Performance analysis of Laser Communication Systems under atmospheric turbulence: a comparative study of channel models and modulation techniques

Y.D. Safitri [1], A.S. Nasution [1], Suhermanto [1], H. Gunawan [1], D.N.S. Sirin [1], A. Indradjad [1], Supriyono [1], A. Maryanto [1], Musyarofah [1], M. Soleh [1], A. Dempster [2]

[1] Research Center for Satellite Technology, National Research and Innovation Agency (BRIN), Bogor 16310, Indonesia;
[2] School of Electrical Engineering and Telecommunications, University of New South Wales, Sydney 2052, Australia

Abstract

This study examines Probability Density Functions (PDFs) of several statistical models–Lognormal, Rayleigh, Gamma-Gamma, Nakagami-m, Rice, and Negative Exponential–in relation to irradiance under weak, moderate, and strong turbulence conditions. Each model exhibits unique characteristics crucial to Free-Space Optical (FSO) communication performance. Lognormal distribution suggests a high probability of low irradiance values, while Rayleigh and Rice show bell-shaped curves. Gamma-Gamma and Nakagami-m offer greater flexibility, displaying moderate peaks and gradual declines. Negative Exponential distribution shows a rapid decay, particularly in random scattering scenarios. Bit Error Rate (BER) performance is evaluated based on instantaneous signal-to-noise ratio (SNR(I)) for various modulation schemes. Among these, 16-Pulse Position Modulation (16-PPM) proves the most robust, followed by Binary Phase Shift Keying (BPSK) and 8-Phase Shift Keying (8-PSK), which also demonstrate strong performance. Differential Phase Shift Keying (DPSK) and 16-Quadrature Amplitude Modulation (16-QAM) offer a balance between performance and spectral efficiency, while 4-Pulse Amplitude Modulation (4-PAM) is highly sensitive to noise. The study reveals that Rayleigh and Rice distributions perform poorly in moderate and strong turbulence, while Nakagami-m and Gamma-Gamma perform better, with Gamma-Gamma excelling in weak and strong turbulence, and Nakagami-m in moderate conditions. At higher SNR(I) levels, BER performance converges across models, minimizing the impact of channel model on modulation scheme's performance.

Keywords: Optical, laser, FSO, channel model, modulation, turbulence.

Citation: Safitri YD, Nasution AS, Suhermanto, Gunawan H, Sirin DNS, Indradjad A, Supriyono, Maryanto A, Musyarofah, Soleh M, Dempster A. Performance analysis of Laser Communication Systems under atmospheric turbulence: a comparative study of channel models and modulation techniques. Computer Optics 2025; 50 (1): 1681. DOI: 10.18287/COJ1681.

Introduction

Radio Frequency (RF) waves are key in space communications, but optical laser links provide a faster alternative. Operating at around 1550 nm (193.5 THz), they support higher data rates and achieve signal-to-noise ratios (SNR) up to 6,000 times higher than Ka-band frequencies, requiring smaller apertures for greater efficiency in spacecraft and ground stations [1 – 2]. Space research organizations and educational institutions are investing in optical ground stations (OGS) to improve access to space laser communication technology. An example is National Aeronautics and Space Administration (NASA)'s Laser Communications Relay Demonstration (LCRD) project, initiated on December 7, 2021 [3 – 4]. The University of Western Australia (UWA)'s Western Australian Optical Ground Station (WAOGS-1), the first OGS in southern hemisphere, is also another example [5].

Once Line of Sight (LOS) is established, laser communication meets demands for high-speed, low-latency data, especially for downlink. However, perfect LOS is unachievable, making pointing, acquisition, and tracking critical due to optical link's strong directivity and small beam divergence [6 – 7]. Atmospheric factors should also be considered because there are various types of turbulence in relation to space optical links.

Free-Space Optical Communication (FSO) uses laser technology to connect urban and rural areas, as well as satellites. It provides benefits like energy harvesting, enhanced security, and high bandwidth for efficient data transmission. Related study in [8] investigates communication systems, focusing on bit-error-rate (BER), link margin, and channel capacity. It assesses SNR of differential phase shift keying (DPSK) modulation using avalanche photodiodes (APD) under atmospheric turbulence with a gamma-gamma distribution model. Additional studies in [9] and [10] investigate the impact of near-sun pointing on optical link performance. Another study in [11] compares FSO communication link performance using On-Off Keying (OOK), Binary Phase Shift Keying (BPSK), DPSK, Quadrature Phase Shift Keying (QPSK), and 8-Phase Shift Keying (8-PSK) modulation formats under strong atmospheric turbulence, utilizing gamma-gamma as channel model for evaluation.

Review in [12] analyzes 12 channel models, highlighting issues in FSO systems, such as weak signal strength from attenuation and scintillation. It finds that Quadrature Amplitude Modulation (QAM) in 16-QAM and 64-QAM outperform

other modulation techniques in Gamma-Gamma and Exponential Weibull models. Review in [13] discusses nine FSO channel models, highlighting turbulence, absorption, and scattering as challenges, emphasizing effective mitigation techniques for improved communication quality while Probability Density Function (PDF) of some channel models (Rayleigh, log-normal, Rician, Nakagami-m, gamma-gamma) are used in [14]. Channel models such as Rayleigh, Log-normal, Rician, and Nakagami-m are suitable for weak to strong turbulence, while Gamma-Gamma performs well across all turbulence conditions. Negative exponential is valid within same range as Gamma-Gamma but excels in negative regions.

Turbulence modeled with normal distribution is explored in [15]. Atmospheric turbulence causes constant light intensity flicker, with intensity and phase fluctuating randomly. Results indicate that receiving aperture size significantly impacts the transmission performance of optical communication systems in atmospheric choke channels. Study in [16] compares BER performance of FSO communication using OOK and BPSK modulation under atmospheric turbulence. It models received irradiance using a gamma-gamma distribution and applies a negative exponential distribution for severe turbulence, showing BPSK's superior performance.

In [17], error performance of DPSK satellite-to-ground laser communication is analyzed under atmospheric turbulence and pointing errors modeled with a gamma-gamma distribution. DPSK modulation helps mitigate performance degradation caused by turbulence and increasing zenith angles. Research in [18] surveys FSO systems, discussing advantages, disadvantages, and applications. It covers modulation techniques like OOK, BPSK, and DPSK, analyzing how atmospheric conditions degrade performance while reviewing various channel models and atmospheric scintillation.

Research in [19] analyzes free-space laser communication performance, focusing on average optical intensity, scintillation effects, and average BER. Larger receiver apertures improve optical power, but increased turbulence worsens BER [20]. Meanwhile, research [21] investigates modulation schemes for FSO systems in challenging South African weather, analyzing power efficiency, bandwidth efficiency, BER, and SNR performance to identify optimal choices.

Building on previous research, this study aims to optimize space laser link performance by exploring combinations of channel models and modulation techniques. It focuses on turbulence-induced scintillation challenges, as its effects are more significant than beam wandering, enhancing overall system performance [12, 22]. This study examines how different channel models and modulation techniques impact space laser link performance under turbulence. It focuses on comparative study for performance evaluation of various channel models and modulation techniques under atmospheric turbulence conditions. The findings expand knowledge and can guide the design of future laser communication systems for both space and terrestrial use.

1. Methods

Weather, atmospheric pressure, and temperature significantly impact FSO communication system performance [23]. While FSO offers advantages, it is vulnerable to atmospheric turbulence, scattering, and attenuation [11]. Scintillation, similar to fading in wireless communication, arises from random refractive index changes due to temperature and pressure variations, causing intensity fluctuations in the wave [13].

1.1. Channel Model

1.1.1. Gamma-gamma

Gamma-Gamma is popular for varying atmospheric turbulence conditions, assuming turbulence consists of large-scale (refraction) and small-scale (scattering) eddies, as defined by modified Rytov theory [11, 14, 27]. Distribution of gamma-gamma is given by formula (1) to (5),

$$f(I) = \frac{2(\alpha\beta)^{\frac{\alpha+\beta}{2}}}{\Gamma(\alpha)\Gamma(\beta)} (I)^{\frac{\alpha+\beta}{2}-1} K_{\alpha-\beta}\left(2\sqrt{\alpha\,\beta\,I}\right), I \geq 0 \tag{1}$$

$$\alpha = \left(\exp\left[\frac{0.49\sigma_r^2}{\left(1+1.11\sigma_r^{\frac{12}{5}}\right)^{\frac{7}{6}}} \right] - 1 \right)^{-1} \tag{2}$$

$$\beta = \left(\exp\left[\frac{0.51\sigma_r^2}{\left(1+0.69\sigma_r^{\frac{12}{5}}\right)^{\frac{5}{6}}} \right] - 1 \right)^{-1} \tag{3}$$

$$\sigma_r^2 = 1.23\, C_n^2\, k^{\frac{7}{6}}\, L^{\frac{11}{6}} \tag{4}$$

$$C_n^2(h) = 0.00594 \left(\frac{w}{27}\right)^2 (10^{-5}h)^{10} \exp\left(-\frac{h}{1000}\right) + 2.7 \times 10^{-16} \exp\left(-\frac{h}{1500}\right) + A\exp\left(-\frac{h}{100}\right) \tag{5}$$

Where f(I) is PDF function in range of irradiance I, $K_n(.)$ is modified second kind Bessel function of n-th order, and α and β are the effective numbers of small and large scales eddies of scattering process [13]. σ_r^2 is Rytov variance indicating the

intensity of air turbulence for slant path optical communication, Γ(·) is gamma function, $C_n^2(h)$ is altitude (h) dependent refractive index structure determining turbulence strength and varies from 10^{-13} to $10^{-17}m^{-2/3}$ for strong to weak turbulence [24]. L is transmission length between transmitter and receiver. "A" and "w" are nominal value of the refractive-index structure parameter at the ground ($m^{-2/3}$) and mean square value of wind speed (m/s), while k is optical wavenumber ($k = 2\pi/\lambda$). Parameters that used in calculation are shown in Tab. 1.

Tab. 1. Calculation Parameters [8, 31, 32]

Parameters	**Symbol**	**Value**
Temperature	Te	300 Kelvin
Bit time	Ts	10 ns
Diameter of optical receiver	D_R	80 mm
Effective receiving area	A_R	0.004021239 m^2
Quantum efficiency	η_Q	0.72
Electronic charge constant	q	1.6×10^{-19} coulomb
Plank's constant	*h*	6.63×10^{-34} Js
Boltzmann's constant	κ	1.38×10^{-13} J/K
Optical beam frequency	f_{op}	193.5 THz
Ionization coefficient ratio	k_{eff}	0.05
APD Gain factor	G	30
APD dark current	I_{dc}	40 nA
Load resistance	R_L	1 kΩ
Receiver field of view	Ω_{FoV}	20 μrad
Receiver efficiency	η_R	0.8
Optical filter transmittance	η_{filter}	0.6
Diameter of optical receiver	D_R	80 mm
Effective receiving area	A_R	0.004021239 m^2
Bandwidth of the optical bandpass filter	$\Delta\lambda_{filter}$	2 nm
Sky spectral radiance	L_λ	0.015 W/cm^2
Sun spectral radiance	I_λ	0.027 W/cm^2
Irradiance	I	0.01 to 5
Transmission Length	L	20000 meters
Altitude for dependent refractive index structure	h	500 meters
The mean square value of the wind speed	w	Weak = 10 m/s Moderate = 21 m/s Strong = 32 m/s
Nominal value of the refractive-index structure parameter at the ground	A	Weak = 8.5×10^{-15} $m^{-2/3}$ Moderate = 1.7×10^{-14} $m^{-2/3}$ Strong = 10^{-13} $m^{-2/3}$
Fixed instantaneous Signal to Noise Ratio	SNR(I)	1 to 30 dB

1.1.2. Lognormal

Log-normal is commonly used for weak atmospheric conditions at short distance. However, it provides inaccurate performance in the tails of data [12]. PDF of Log-Normal distribution is given in equation (6) [13] where I_i is irradiance in the absence of turbulence which is set to 1, while scintillation index is denoted as σ_r^2 in formula (4).

$$f(I) = \frac{1}{(2\pi\sigma_r^2)^{1/2}} \exp\left\{ -\frac{\ln\left[\left(\frac{I}{I_i}\right)+\left(\frac{\sigma_r^2}{2}\right)\right]^2}{2\sigma_r^2} \right\}, I \geq 0 \quad (6)$$

1.1.3. Rayleigh

Rayleigh is also used to estimate channel model. In case of Rayleigh, scintillation index is 1. At low (deeply faded) values, Rayleigh density function is more concentrated [14]. PDF of Rayleigh distribution is given by equation (7) [12, 25], where Ω value is substituted with σ_r^2.

$$f(I) = \frac{2I}{\Omega} \exp\left(-\frac{I^2}{\Omega}\right), I \geq 0 \quad (7)$$

1.1.4. Nakagami-m

Nakagami-m distribution is a statistical model linked to Gamma-Gamma distribution and derived from Chi distribution. It features two parameters, spread Ω and shape parameter *m*, enabling better performance than Rayleigh and Rician [12]. Formula can be seen in equation (8) [25], where *m* is Nakagami-m fading parameter which set to 0.5, while Ω is substituted with σ_r^2.

$$f(I) = \frac{2\mathrm{m}^{\mathrm{m}} I^{2\mathrm{m}-1}}{\Omega^{\mathrm{m}}\Gamma^{\mathrm{m}}} \exp\left(-\frac{\mathrm{m}I^2}{\Omega}\right), \mathrm{I} \geq 0 \quad (8)$$

1.1.5. Nakagami-n (Rice)

Nakagami-n or Rice distribution is often used to model propagation paths with many random weaker components and one strong direct LOS component. Formula is displayed in equation (9) [25 – 26], where n is Nakagami-n fading parameter which set to 0 and where I_0 is the zeroth-order modified Bessel function of the first kind.

$$f(I) = \frac{2(1+\mathrm{n}^2)\mathrm{e}^{-\mathrm{n}^2} I}{\Omega} \exp\left(-\frac{(1+\mathrm{n}^2)I^2}{\Omega}\right) \mathrm{I}_0\left(2\mathrm{n}\,\mathrm{I}\sqrt{\frac{1+\mathrm{n}^2}{\Omega}}\right), \mathrm{I} \geq 0 \quad (9)$$

1.1.6. Negative Exponential

Negative exponential is used for large variations in atmospheric irradiance, particularly in saturation regimes. It performs well when scattering particles outnumber laser wavelengths but has disadvantage of an ideal value in negative region [12]. The equation is given in expression (10), where I_N is mean of irradiance. When generating PDF, I_N is substituted with σ_r^2 to see the effect of scintillation in this model.

$$f(I) = \frac{1}{I_N} exp\left\{-\frac{I}{I_N}\right\}, I \geq 0 \quad (10)$$

1.2. Modulation Technique

Modulation techniques that were used in this investigation are described in explanation below.

1.2.1. On-Off Keying (OOK)

OOK scheme is popular in commercial terrestrial FSO communication systems due to its ease of use and adaptability [21]. It transmits bits 0 and 1 using either Non-Return-Zero (NRZ) or Return-Zero (RZ) waveforms. Formula (11) shows BER for NRZ-OOK, while formula (12) illustrates BER of RZ-OOK as function of Signal-to-Noise Ratio (SNR). Shorter pulse duration of RZ-OOK enhances power efficiency but requires higher transmission capacity [21].

$$\mathrm{p}_{\mathrm{e,NRZ-OOK}} = \frac{1}{2}\mathrm{erfc}\left(\frac{1}{2\sqrt{2}}\sqrt{\mathrm{SNR}}\right) \quad (11)$$

$$\mathrm{p}_{\mathrm{e,RZ-OOK}} = \frac{1}{2}\mathrm{erfc}\left(\frac{1}{2}\sqrt{\mathrm{SNR}}\right) \quad (12)$$

1.2.2. Differential Phase Shift Keying (DPSK)

DPSK relative phase modulation model uses the phase difference between adjacent symbols to transmit information. Under same BER conditions, NRZ-OOK has twice the average power of DPSK [27]. DPSK equation is given by formula (13).

$$\mathrm{p}_{\mathrm{e,DPSK}} = \frac{1}{2}\mathrm{erfc}\left(\frac{\sqrt{\mathrm{SNR}}}{\sqrt{2}}\right) \quad (13)$$

1.2.3. Binary Phase Shift Keying (BPSK)

BPSK is the simplest PSK and is more resilient to noise than OOK as NRZ-OOK may require up to twice the power of BPSK to achieve same BER performance [27]. Formula for BPSK error rate is given by equation (14).

$$\mathrm{p}_{\mathrm{e,BPSK}} = \frac{1}{2}\mathrm{erfc}\left(\sqrt{\mathrm{SNR}}\right) \quad (14)$$

1.2.4. Quadrature Phase Shift Keying (QPSK)

QPSK combines two bits into signals, using four specific phases for transmission, it is another way to increase spectral efficiency. It enhances spectral efficiency and can be viewed as two BPSK orthogonal signals [27]. Error rate for QPSK is determined by equation (15).

$$\mathrm{p}_{\mathrm{e,QPSK}} = \mathrm{erfc}\left(\sqrt{\mathrm{SNR}}\right) \quad (15)$$

1.2.5. 8-Phase Shift Keying (8-PSK)

8-PSK boosts data rates over BPSK and QPSK by encoding more bits per symbol but demands a higher signal-to-noise ratio due to smaller phase differences between symbols. Equation (16) provides error rate for 8-PSK.

$$\mathrm{p}_{\mathrm{e,8-PSK}} = 2\mathrm{erfc}\left(\sqrt{\mathrm{SNR}}\right) \quad (16)$$

1.2.6. 16-Pulse Position Modulation (16-PPM)

16-PPM allows a laser pulse to represent multiple bits by positioning it within a symbol duration equal to the number of bits. This also eliminates decision threshold dependence on input power [28]. Error rate for 16-PPM can be determined using equation (17).

$$p_{e,16-PPM} = \frac{1}{2}\text{erfc}\left(2\sqrt{SNR}\right) \quad (17)$$

1.2.7. 16-Quadrature Amplitude Modulation (16-QAM)

As two quadrature carriers are used in QAM modulation to transmit signals, a symbol of four bits, or 2^N where N = 4, will be used to transmit sixteen possible bits. Thus, two potentially distinct symbols can be produced using QAM [29, 30]. Error rate for 16-QAM is defined by equation (18).

$$p_{e,16-QAM} = \frac{3}{8}\text{erfc}\left(\frac{2\sqrt{SNR}}{\sqrt{10}}\right) \quad (18)$$

1.2.8. 4-Pulse Amplitude Modulation (4-PAM)

A type of signal modulation known as pulse amplitude modulation encodes message information in amplitude of a sequence of signal pulses [28]. Equation (19) defines error rate for 4-PAM.

$$p_{e,4-PAM} = \frac{1}{2}\text{erfc}\left(\frac{\sqrt{SNR}}{6}\right) \quad (19)$$

To estimate the PDF and generate the BER, following steps are adopted, with parameters described in Tab. 1.
Step 1. Calculate PDF in every channel model;
Step 2. Calculate atmospheric turbulence from equation;
(4) and equation (5);
Step 3. Calculate error rate from various modulation using;
fixed SNR value range and PDF for every channel model.
Variations in atmospheric turbulence intensity affect BER performance. Equation (20) defines instantaneous electrical SNR in terms of received irradiance (I) to compute the average BER [8].

$$SNR(I) = \frac{[GR_d(A_R I + P_b) + I_{dc}]^2}{\frac{2G^2 q R_d F(A_R I + P_b)}{T_s} + \frac{4\kappa T_e}{T_s R_L}} \quad (20)$$

where G is APD gain, R_d is detector responsivity $\left(R_d = \eta_Q q/hf_{op}\right)$, where η_Q is quantum efficiency, h is Plank's constant, and f_{op} is optical beam frequency. A_R is effective receiving area (area of circle), I is irradiance, P_b is background noise power, I_{dc} is dark current, q is electronic charge, F is excess noise factor where $F = k_{eff}G + (1 - k_{eff})(2 - 1/G)$, and k_{eff} is ionization coefficient ratio. T_s is bit time, κ is Boltzmann's constant, T_e is temperature, R_L is load resistance. While background noise from sky and sun itself is expressed in below equations [8].

$$P_b = P_{sky} P_{sun} \quad (21)$$
$$P_{sky} = L_\lambda \Omega_{FoV} \eta_R \eta_{filter} A_R \Delta\lambda_{filter} \quad (22)$$
$$P_{sun} = I_\lambda \Omega_{FoV} \eta_R \eta_{filter} A_R \Delta\lambda_{filter} \quad (23)$$

Equation (20) to (23) are used to calculate SNR(I) with diameter (D_R) of 8 to 20 cm for optical receiver and got very high SNR(I) value in range of more than 60 dB so BER graph does not appear in simulation because of very near-zero results. Thus, to show the BER graph, a fixed SNR value ranging from 0 to 30 dB is used, as indicated in the last line of Tab. 1. New error rate formula for modulations, utilizing PDF values are expressed in equations (24) to (32) [11, 28].

$$p_{e,DPSK} = \int_0^\infty f(I)\left[\frac{1}{2}\text{erfc}\left(\frac{\sqrt{SNR(I)}}{\sqrt{2}}\right)\right] dI \quad (24)$$
$$p_{e,BPSK} = \int_0^\infty f(I)\left[\frac{1}{2}\text{erfc}\left(\sqrt{SNR(I)}\right)\right] dI \quad (25)$$
$$p_{e,QPSK} = \int_0^\infty f(I)\left[\text{erfc}\left(\sqrt{SNR(I)}\right)\right] dI \quad (26)$$
$$p_{e,8-PSK} = \int_0^\infty f(I)\left[2\text{erfc}\left(\sqrt{SNR(I)}\right)\right] dI \quad (27)$$
$$p_{e,NRZ-OOK} = \int_0^\infty f(I)\left[\frac{1}{2}\text{erfc}\left(\frac{1}{2\sqrt{2}}\sqrt{SNR(I)}\right)\right] dI \quad (28)$$
$$p_{e,RZ-OOK} = \int_0^\infty f(I)\left[\frac{1}{2}\text{erfc}\left(\frac{1}{2}\sqrt{SNR(I)}\right)\right] dI \quad (29)$$
$$p_{e,16-PPM} = \int_0^\infty f(I)\left[\frac{1}{2}\text{erfc}\left(2\sqrt{SNR(I)}\right)\right] dI \quad (30)$$
$$p_{e,16-QAM} = \int_0^\infty f(I)\left[\frac{3}{8}\text{erfc}\left(\frac{2\sqrt{SNR(I)}}{\sqrt{10}}\right)\right] dI \quad (31)$$
$$p_{e,4-PAM} = \int_0^\infty f(I)\left[\frac{1}{2}\text{erfc}\left(\frac{\sqrt{SNR(I)}}{6}\right)\right] dI \quad (32)$$

2. Results and Discussions

This paper examines three turbulence calculation schemes (weak, moderate, and strong wind) over a 20 km transmission length (L). As shown in Tab. 1 and equations (4) and (5), these turbulence states depend on the wind speed's mean

square value (w) and ground-level refractive index structure parameter (A), which together influence turbulence intensity. Altitude (h) of the refractive index structure within the atmospheric boundary layer (0 – 3 km) is also critical; a higher h improves BER, with 500 meters used in this study to optimize turbulence without significantly degrading the transmitted signal. A 20 km length is chosen because longer distances lead to higher BER values, indicating decreased link performance, similar to the effect of altitude on the refractive index structure.

2.1. PDF for channel model in different turbulence state

Fig. 1, 2 and 3 respectively provide a comparative analysis of statistical models under weak, moderate, and strong turbulence conditions, illustrating their effects on irradiance. Fig. 1 compares Lognormal, Rayleigh, Gamma-Gamma, Nakagami-m, Rice, and Negative Exponential models. Lognormal shows a high probability of low irradiance, with a steep rise followed by a gradual decline. Rayleigh and Rice exhibit overlapping bell-shaped curves peaking at moderate irradiance, while Gamma-Gamma suggests a mode slightly above zero, indicating moderate values. Nakagami-m shows a similar, less pronounced pattern, reflecting flexibility across turbulence regimes. Negative Exponential decreases rapidly, indicating a higher likelihood of lower irradiance values without a dominant trend.

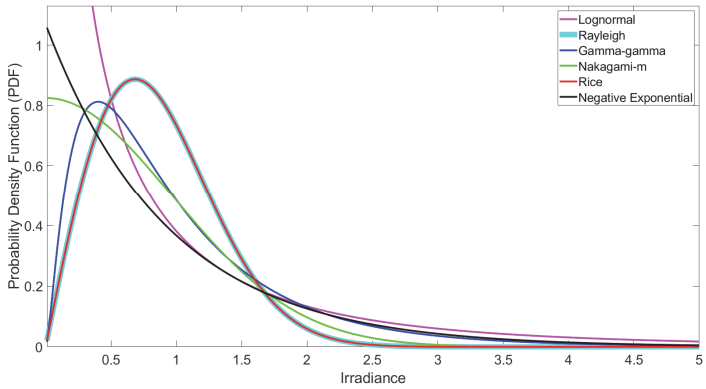

Fig. 1. PDF vs Irradiance for Weak Turbulence

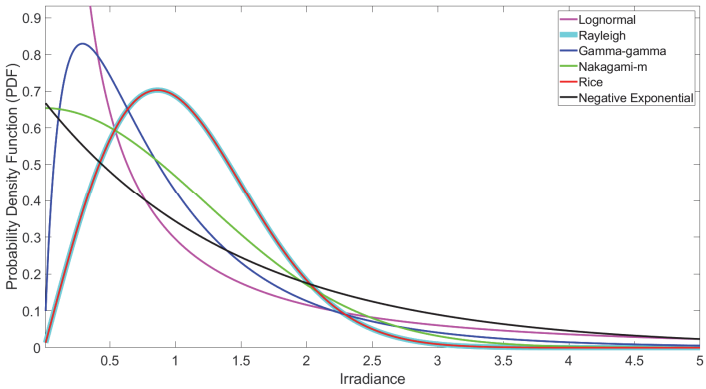

Fig. 2. PDF vs Irradiance for Moderate Turbulence

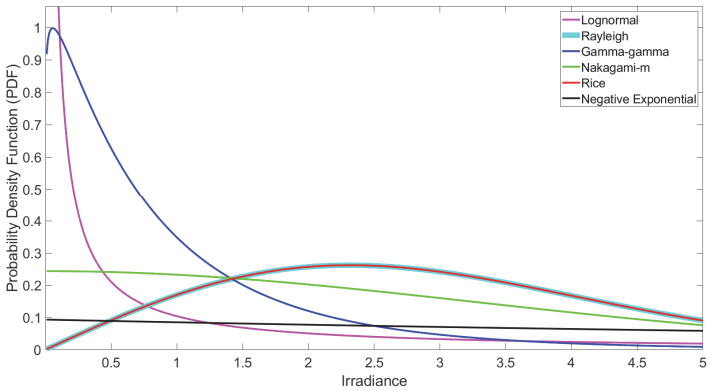

Fig. 3. PDF vs Irradiance for Strong Turbulence

Fig. 2 further compares these models. Lognormal distribution rises sharply and falls steeply, indicating a concentration of lower irradiance values. Rayleigh and Rice maintain symmetric bell-shaped patterns, peaking at moderate irradiance. Gamma-Gamma has the highest peak, reflecting its effectiveness in moderate turbulence. Nakagami-m shows a moderate

peak, highlighting adaptability, while Negative Exponential exhibits a rapid decline, indicating random scattering with no central tendency.

Fig. 3 highlights pronounced differences between models. Lognormal distribution rises sharply and falls quickly, reflecting weak to moderate turbulence. Rayleigh and Rice have lower peaks than before. Gamma-Gamma shows higher peak at lower irradiance. Nakagami-m has relatively flat curve, while Negative Exponential continues its steady decline, representing random scattering. Understanding these statistical models is crucial for enhancing the performance and reliability of optical communication systems in varying turbulence conditions.

2.2. BER performance in different modulations

Fig. 4 compares BER performance of different modulation schemes under strong turbulence (Gamma-Gamma distribution), highlighting each scheme's ability to handle noise and maintain low BER as SNR(I) increases.

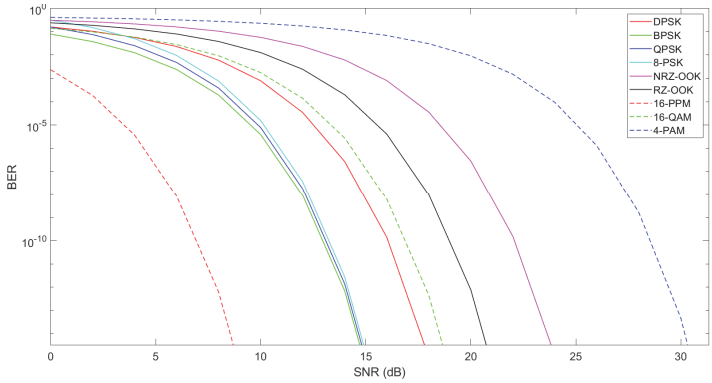

Fig. 4. BER vs SNR(I) for Strong Turbulence in Gamma-gamma

All modulation schemes exhibit similar patterns under turbulence, but 16-PPM is particularly robust, showing a sharp decrease in BER with increasing SNR(I), making it ideal for high-reliability scenarios in noisy environments. BPSK and 8-PSK perform closely behind 16-PPM, with BPSK being favored for its simplicity and reliability. DPSK and 16-QAM strike a balance between performance and spectral efficiency, achieving lower BER at moderate SNR(I) compared to NRZ-OOK and RZ-OOK, which require higher SNR(I) for similar results. OOK, while simple, is less efficient in turbulence than phase-shift keying schemes. 4-PAM is the most noise-sensitive, needing much higher SNR(I) for comparable BER, making it less robust in turbulent conditions.

In summary, 16-PPM is the best option for strong turbulence, providing the lowest BER at lower SNR values, followed by BPSK and 8-PSK. DPSK and 16-QAM offer a good balance of performance and efficiency, while 4-PAM struggles in noisy conditions. The channel model affects BER only when channel parameters vary from zero to infinity, highlighting each scheme's sensitivity to channel conditions. Choosing the right modulation scheme is crucial based on the expected environment.

Going further, BER values for different combinations channel model across fixed SNR(I) range are also investigated. The data suggests regardless of the model, BER tends to converge, indicating minimal impact from the choice of modulation technique. For example, BER values for the combinations of Gamma-gamma with Rayleigh, Nakagami, Rice, or Negative Exponential are nearly identical, consistently decreasing with increasing SNR(I). Although the Gamma-gamma with Lognormal combination starts with a higher BER, it eventually converges to values similar to the other models at high SNR(I). This consistency across different turbulence models indicates that BER performance is reliable regardless of the channel model used.

Tab. 2 in Appendix A presents detailed BER values for strong turbulence across different modulation schemes. To generate these results, equations (24) to (32) were used, with upper integral limit set to 1 for clearer comparisons among channel models. In weak turbulence, Negative Exponential consistently outperforms others across all modulations, followed closely by Gamma-Gamma, Rayleigh, and Rice, which yield similar results. Nakagami ranks next, while Lognormal is the least effective. In moderate turbulence, Negative Exponential, Rayleigh, and Rice provide the best performance, followed by Nakagami and Gamma-Gamma, with Lognormal again being the worst. In strong turbulence as shown in Table 2, the performance pattern mirrors that of moderate turbulence, with similar rankings for all models.

Additionally, an investigation into PPM modulation was conducted to evaluate the effect of channel model on this modulation type. PPM was chosen for its proven superior performance across all channel models compared to other modulation schemes mentioned. BER equations for various PPM schemes are detailed in formulas (33) to (35) [28].

$$\mathrm{p_{e,NRZ-OOK}} = \int_0^\infty f(I)\left[\frac{1}{2}\mathrm{erfc}\left(\frac{1}{2\sqrt{2}}\sqrt{\mathrm{SNR(I)}}\right)\right]dI \tag{33}$$

$$\mathrm{p_{e,NRZ-OOK}} = \int_0^\infty f(I)\left[\frac{1}{2}\mathrm{erfc}\left(\frac{1}{\sqrt{2}}\sqrt{\mathrm{SNR(I)}}\right)\right]dI \tag{34}$$

$$\mathrm{p_{e,NRZ-OOK}} = \int_0^\infty f(I)\left[\frac{1}{2}\mathrm{erfc}\left(\frac{\sqrt{3}}{\sqrt{2}}\sqrt{\mathrm{SNR(I)}}\right)\right]dI \tag{35}$$

Fig. 5 shows PPM results in strong turbulence, confirming that Negative Exponential, Rayleigh, and Rice outperform other models, while Nakagami, Gamma-Gamma, and Lognormal perform slightly lower. The analysis of PPM schemes shows that 16-PPM consistently delivers the best performance, followed closely by 8-PPM, which remains robust. In contrast, 4-PPM and 2-PPM rank lower, with higher BER values highlighting the advantages of higher-level PPM schemes.

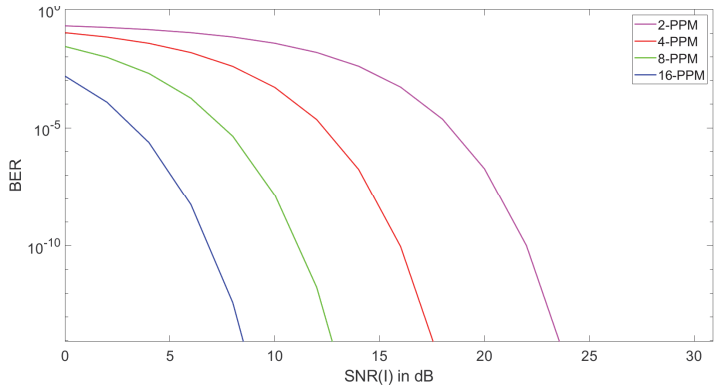

Fig. 5. BER vs SNR(I) for Strong Turbulence in Gamma-gamma for PPM

The behavior of Rayleigh and Rice in relation to BER results aligns with their PDF patterns, consistently overlapping and producing identical values under the same conditions. However, they struggle to capture characteristics in moderate and strong turbulence due to similarities with Negative Exponential. In contrast, Lognormal shows the poorest performance across all turbulence levels. Nakagami and Gamma-Gamma emerge as more effective alternatives, with Gamma-Gamma excelling in weak and strong turbulence, while Nakagami leads in moderate turbulence, indicating that each model has strengths depending on turbulence levels.

Overall, Rayleigh and Rice offer some insights, but Nakagami and Gamma-Gamma provide more reliable BER results across conditions, highlighting the importance of selecting the right model for optimal communication system performance.

Conclusions

The analysis of BER values and PDF performance under varying turbulence conditions offers crucial insights for optimizing optical communication systems. Across different channel models, BER values converge similarly across modulation schemes, with minimal impact from modulation technique. In strong Gamma-Gamma turbulence, 16-PPM shows the highest robustness, followed by BPSK and 8-PSK, while DPSK and 16-QAM have balance in performance and spectral efficiency. This reliability across turbulence models highlights system versatility, with Gamma-Gamma excelling in weak and strong turbulence, while Nakagami performing best in moderate conditions. Rayleigh and Rice distributions, though yielding similar values, are less effective in moderate and strong turbulence scenarios.

Acknowledgements

The authors express their gratitude to BRIN's Research Center for Satellite Technology, the University of Indonesia, and the University of New South Wales for providing essential resources for this study.

References

[1] Roberts, W. T., D. Antsos, A. Croonquist, S. Piazzolla, L. C. Roberts, V. Garkanian, T. Trinh, M. W. Wright, R. Rogalin, J. Wu, and L. Clare, (2016) Overview of Ground Station 1 of the NASA Space Communications and Navigation Program, Proc. of 2016 SPIE 9739, Free-Space Laser Communication and Atmospheric Propagation XXVIII, San Francisco, California, United States, 1-18. DOI: 10.1117/12.2217465.

[2] Ronny, A. T. Y., T. V. Huynh, and B. N. Agrawal, (2012) Link Performance Analysis of A Ship-to-Ship Laser Communication System, Thesis, Naval Postgraduate School Monterey, California.

[3] Edwards, B. L., D.J. Israel, and S. K. Vithlani, (2018) Latest Changes to NASA's Laser Communications Relay Demonstration Project, Proc. of 2018 SPIE 10524, Free-Space Laser Communication and Atmospheric Propagation XXX, San Francisco, California, United States, 1-11. DOI: 10.1117/12.2285221.

[4] Schauer, K., (2021) 6 Things You Need to Know about NASA's Laser Communications Relay Demonstration, NASA, USA.

[5] Walsh, S., A. Frost, W. Anderson, T. Digney, B. D. Matthews, D. Gozzard, C. Gravestock, L. Howard, S. Karpathakis, A. McCann, and S. Schediwy, (2022) The Western Australian Optical Ground Station, Proc. of 2021 International Communications Satellite Systems Conference, Arlington, Virginia, USA, 1-8. DOI: 10.48550/arXiv.2201.11846.

[6] Nikulin, V. V., and R. Khandekar, (2005) "Performance of Laser Communication Uplinks and Downlinks in the Presence of Pointing Errors and Atmospheric Distortions, Proc. of 2005 SPIE 5712, Free-Space Laser Communication Technologies XVII, San Jose, California, United States, 37-45. DOI: 10.1117/12.589678.

[7] Liu, R., S. Duan, H. Sun, and L. Zhang, (2019) Performance Analysis of Laser Communication Based on Circular Polarization Modulating-Reflector, Proc. of 2019 IEEE 4th Advanced Information Technology, Electronic and Automation Control Conference, Chengdu, China, 218-221. DOI: 10.1109/IAEAC47372.2019.8998064.

[8] Lim, H. C., Jong U. P., Mansoo C., Chul S. C., Jae D. C., and Jongah K., (2020) "Performance Analysis of DPSK Optical Communication for LEO-to-Ground Relay Link Via a GEO Satellite," Astronomy and Space Sciences 37 (1), 11–18. DOI: 10.5140/JASS.2020.37.1.11.
[9] Biswas, A., F. Khatri, and D. Boroson, (2006) Near-Sun Free-Space Optical Communications from Space, Proc. of 2006 IEEE Aerospace Conference, Big Sky, MT, USA, 1-9. DOI: 10.1109/AERO.2006.1655849.
[10] Mohageg, M., M. C. Lorio, D. J. Hoppe, J. N. Huleis, A. Abramovici, and S. K. Chung, (2020) Minimizing Effect of Sun-Earth-Probe Angle for RF / Optical Hybrid Telescope, Proc. of 2020 SPIE 11272, Free-Space Laser Communications XXXII, San Francisco, California, United States, 1-8. DOI: 10.1117/12.2551066.
[11] Choyon, A. K. M. S. J., and R. Chowdhury, (2020) "Performance Comparison of Free-Space Optical (FSO) Communication Link Under OOK, BPSK, DPSK, QPSK and 8-PSK Modulation Formats in the Presence of Strong Atmospheric Turbulence," Optical Communications 44 (1), 1-7. DOI: 10.1515/joc-2019-0250.
[12] Anandkumar, D., and R. G. Sangeetha, (2021) "A Survey on Performance Enhancement in Free Space Optical Communication System through Channel Models and Modulation Techniques," Optical and Quantum Electronics 53 (5), 1-39. DOI: 10.1007/s11082-020-02629-6.
[13] Anbarasi, K., C. Hemanth, and R. G. Sangeetha, (2017) "A Review on Channel Models in Free Space Optical Communication Systems," Optics and Laser Technology 97, 161-171. DOI: 10.1016/j.optlastec.2017.06.018.
[14] Barua, B., M. M. Hossain, M. R. Islam, and M. K. Bashar, (2011) "Performance Evaluation of Different Type of Channel Models in FSO Communication," International Journal of Science and Advanced Technology 1 (5), 116-122.
[15] Liu, X., (2019) Research on Transmission Performance of Laser Communication System in Atmospheric Turbulent Channel, Proc. of the 2019 3rd International Conference on Mechatronics Engineering and Information Technology, Dalian, China, 137-142. DOI: 10.2991/icmeit-19.2019.24.
[16] Barua, B., (2011) "Comparison the Performance of Free-Space Optical Communication with OOK and BPSK Modulation under Atmospheric Turbulence," International Journal of Engineering Science and Technology 3 (5), 4391-4399.
[17] Hao, S., X. Wan, Q. Zhao, and C. Xu, (2019) Error Performance of DPSK Satellite-to-Ground Laser Communication over Atmospheric Turbulence and Pointing Errors, Proc. of the 2019 2nd International Conference on Advanced Algorithms and Control Engineering, Guilin, China, 1-8. DOI: 10.1088/1742-6596/1213/5/052073.
[18] Kaur, S., and P. Bhardwaj, (2018) "Performance of FSO Communication in the Atmospheric Turbulence for Various Modulation Schemes," International Journal of Engineering Trends and Technology 55 (3), 142-147. DOI: 10.14445/22315381/IJETT-V55P226.
[19] Li, M., L. Tan, J. Ma, S. Yu, S. Zhai, and J. Wu, (2015) "Performance Analysis of a Free-Space Laser Communication System with a Gaussian-Schell Model," Modern Optics 62 (19), 1608-1615. DOI: 10.1080/09500340.2015.1054907.
[20] Walther, F. G., S. Michael, R. R. Parenti, and J. A. Taylor, (2010) Air-to-Ground Lasercom System Demonstration Design Overview and Results Summary" Proc. of 2010 SPIE 7814, Free-Space Laser Communications X, San Diego, California, United States, 1-9. DOI: 10.1117/12.864262.
[21] Maswikaneng, S. P., P. A. Owolawi, S. O. Oio, M. I. Mphahlele, and Z. L. Mahlobogwane, (2021) Investigation of Different Modulation Techniques under Strong FSO Turbulance Channel in South Africa." Proc. of 2020 Asia Conference on Computers and Communications, Singapore, Singapore, 75–81. DOI: 10.1109/ACCC51160.2020.9347905.
[22] Wang, T., X. Zhao, Y. Song, J. Wang, X. Yu, and Y. Zhang, (2021) "Atmospheric Laser Communication Technology Based on Detector Gain Factor Regulation Control," IEEE Access 9, 43339-43348. DOI: 10.1109/ACCESS.2021.3061504.
[23] Shaker, F. K., and M. A. A. Ali, (2019) "Performance of Free Space Optical Communication Link under Foggy Weather," Communications 14 (6) 518–523. DOI: 10.12720/jcm.14.6.518-523.
[24] Morio, T., K. Toshiaki, K. Werner, T. Masahiro, T. Hideki, S. Yozo, T. Yoshihisa, K. Yoshisada. K. Hiroo, J. Takashi, Y. Shiro, and A. Katsuyoshi, (2012) "4-2 Overview of the Laser Communication System for the NICT Optical Ground Station and Laser Communication Experiments on Ground-to-Satellite Links," National Institute of Information and Communications Technology 59 (1/2), 53-75.
[25] Simon, M. K., and M. S. Alouini, (2002) Digital Communication over Fading Channels : A Unified Approach to Performance Analysis, 1st ed John Wiley & Sons, United States.
[26] Doukas, A., and G. Kalivas, (2006) Rician K Factor Estimation for Wireless Communication Systems, Proc. of 2006 International Conference on Wireless and Mobile Communications, Bucharest, Romania, 1-5. DOI: 10.1109/ICWMC.2006.81.
[27] Zhang, H., H. Li, X. Dongya, and C. Chao, (2015) "Performance Analysis of Different Modulation Techniques for Free-Space Optical Communication System," Telkomnika 13 (3), 880–888. DOI: 10.12928/telkomnika.v13i3.1976.
[28] Elganimi, T. Y, (2013) "Performance Comparison between OOK, PPM and PAM Modulation Schemes for Free Space Optical (FSO) Communication Systems: Analytical Study," International Journal of Computer Applications 79 (11), 22-27. DOI: 10.5120/13786-1838.
[29] Kayodde, A., and A. Opeyemi, (2017) "BER and SNR Comparisons for 8, 16 and 64 QAM Modulation Schemes through Rain Affected Air Interface Channel," SSRG International Journal of Electrical and Electronics Engineering 4 (6), 1-8. DOI: 10.14445/23488379/IJEEE-V4I6P102.
[30] Pratiwi, W., and E. Setyowati, (2021) "Analisis Perbandingan 16-QAM Dan 64-QAM Pada Kanal AWGN Untuk Sistem Komunikasi Nirkabel," Telecommunications, Networks, Electronics, and Computer Technologies 1 (2), 71-76. DOI: 10.17509/telnect.v1i2.40861.
[31] Liang, J., A. U. Chaudhry, E. Erdogan, and H. Yanikomeroglu, (2022) Link Budget Analysis for Free-Space Optical Satellite Networks, Proc. of 2022 IEEE 23rd International Symposium on a World of Wireless, Mobile and Multimedia Networks, Belfast, United Kingdom, 471-476. DOI: 10.1109/WoWMoM54355.2022.00073.
[32] Li, M., B. Li, X. Zhang, Y. Song, L. Chang, and Y. Chen, (2016) "Investigation of the Phase Fluctuation Effect on the BER Performance of DPSK Space Downlink Optical Communication System on Fluctuation Channel," Optics Communications 366, 248-252. DOI: 10.1016/j.optcom.2016.01.003.

Appendix A

Table. 2. BER value with SNR(I) between (0-16dB) for Strong Turbulence

Modulations	Channel Model	SNR(I) between 0 dB to 16 dB								
		0	2	4	6	8	10	12	14	16
16-PPM	Gamma-gamma	0.00153	0.000121	2.41E-06	5.45E-09	3.94E-13	1.22E-19	6.75E-30	4.24E-46	1.01E-71
	Rayleigh	0.000209	1.65E-05	3.29E-07	7.43E-10	5.38E-14	1.67E-20	9.20E-31	5.77E-47	1.38E-72
	Lognormal	0.017909	0.001416	2.82E-05	6.70E-08	1.13E-12	3.51E-19	1.93E-29	1.21E-45	2.90E-71
	Nakagami-m	0.000562	4.44E-05	8.85E-07	2.00E-09	1.45E-13	4.49E-20	2.48E-30	1.55E-46	3.72E-72
	Negative Exp	0.000209	1.65E-05	3.29E-07	7.43E-10	5.38E-14	1.67E-20	9.20E-31	5.77E-47	1.38E-72
	Rice	0.000209	1.65E-05	3.29E-07	7.43E-10	5.38E-14	1.67E-20	9.20E-31	5.77E-47	1.38E-72
BPSK	Gamma-gamma	0.051448	0.024534	0.008177	0.001562	0.000125	2.53E-06	5.89E-09	4.45E-13	1.48E-19
	Rayleigh	0.007014	0.003345	0.001115	0.000213	1.70E-05	3.45E-07	8.03E-10	6.07E-14	2.02E-20
	Lognormal	0.602233	0.28719	0.095721	0.018288	0.001462	2.96E-05	7.24E-08	1.28E-12	4.25E-19
	Nakagami-m	0.018884	0.009006	0.003002	0.000573	4.58E-05	9.30E-07	2.16E-09	1.64E-13	5.44E-20
	Negative Exp	0.007014	0.003345	0.001115	0.000213	1.70E-05	3.45E-07	8.03E-10	6.07E-14	2.02E-20
	Rice	0.007014	0.003345	0.001115	0.000213	1.70E-05	3.45E-07	8.03E-10	6.07E-14	2.02E-20
QPSK	Gamma-gamma	0.102896	0.049068	0.016355	0.003125	0.00025	5.07E-06	1.18E-08	8.91E-13	2.97E-19
	Rayleigh	0.014027	0.006689	0.00223	0.000426	3.40E-05	6.91E-07	1.61E-09	1.21E-13	4.04E-20
	Lognormal	1.204465	0.574381	0.191442	0.036575	0.002924	5.93E-05	1.45E-07	2.55E-12	8.50E-19
	Nakagami-m	0.037769	0.018011	0.006003	0.001147	9.17E-05	1.86E-06	4.32E-09	3.27E-13	1.09E-19
	Negative Exp	0.014027	0.006689	0.00223	0.000426	3.40E-05	6.91E-07	1.61E-09	1.21E-13	4.04E-20
	Rice	0.014027	0.006689	0.00223	0.000426	3.40E-05	6.91E-07	1.61E-09	1.21E-13	4.04E-20
8-PSK	Gamma-gamma	0.205791	0.098137	0.032709	0.006249	0.0005	1.01E-05	2.36E-08	1.78E-12	5.93E-19
	Rayleigh	0.028055	0.013379	0.004459	0.000852	6.81E-05	1.38E-06	3.21E-09	2.43E-13	8.09E-20
	Lognormal	2.408931	1.148762	0.382883	0.07315	0.005847	0.000119	2.90E-07	5.11E-12	1.70E-18
	Nakagami-m	0.075538	0.036022	0.012006	0.002294	0.000183	3.72E-06	8.65E-09	6.54E-13	2.18E-19
	Negative Exp	0.028055	0.013379	0.004459	0.000852	6.81E-05	1.38E-06	3.21E-09	2.43E-13	8.09E-20
	Rice	0.028055	0.013379	0.004459	0.000852	6.81E-05	1.38E-06	3.21E-09	2.43E-13	8.09E-20
DPSK	Gamma-gamma	0.103783	0.068049	0.036956	0.01505	0.003928	0.000512	2.24E-05	1.76E-07	9.15E-11
	Rayleigh	0.014148	0.009277	0.005038	0.002052	0.000535	6.98E-05	3.06E-06	2.40E-08	1.25E-11
	Lognormal	1.214849	0.796564	0.432594	0.176169	0.045977	0.005993	0.000263	2.12E-06	2.62E-10
	Nakagami-m	0.038094	0.024978	0.013565	0.005524	0.001442	0.000188	8.24E-06	6.47E-08	3.36E-11
	Negative Exp	0.014148	0.009277	0.005038	0.002052	0.000535	6.98E-05	3.06E-06	2.40E-08	1.25E-11
	Rice	0.014148	0.009277	0.005038	0.002052	0.000535	6.98E-05	3.06E-06	2.40E-08	1.25E-11
RZ OOK	Gamma-gamma	0.15683	0.122115	0.08583	0.05177	0.024761	0.00829	0.001595	0.000129	2.66E-06
	Rayleigh	0.02138	0.016647	0.011701	0.007058	0.003376	0.00113	0.000217	1.76E-05	3.63E-07
	Lognormal	1.835805	1.429444	1.004698	0.606006	0.289841	0.097044	0.018672	0.001509	3.12E-05
	Nakagami-m	0.057566	0.044824	0.031505	0.019003	0.009089	0.003043	0.000586	4.73E-05	9.77E-07
	Negative Exp	0.02138	0.016647	0.011701	0.007058	0.003376	0.00113	0.000217	1.76E-05	3.63E-07
	Rice	0.02138	0.016647	0.011701	0.007058	0.003376	0.00113	0.000217	1.76E-05	3.63E-07
NRZ OOK	Gamma-gamma	0.201826	0.173035	0.140019	0.104158	0.068402	0.037236	0.015219	0.003994	0.000525
	Rayleigh	0.027514	0.023589	0.019088	0.014199	0.009325	0.005076	0.002075	0.000545	7.16E-05
	Lognormal	2.362522	2.025496	1.639017	1.219243	0.800696	0.43587	0.178151	0.046758	0.006149
	Nakagami-m	0.074083	0.063514	0.051395	0.038232	0.025108	0.013668	0.005586	0.001466	0.000193
	Negative Exp	0.027514	0.023589	0.019088	0.014199	0.009325	0.005076	0.002075	0.000545	7.16E-05
	Rice	0.027514	0.023589	0.019088	0.014199	0.009325	0.005076	0.002075	0.000545	7.16E-05

Modulations	Channel Model	SNR(I) between 0 dB to 16 dB								
		0	2	4	6	8	10	12	14	16
16-QAM	Gamma-gamma	0.09103	0.063817	0.038345	0.018232	0.006049	0.001147	9.07E-05	1.81E-06	4.09E-09
	Rayleigh	0.01241	0.0087	0.005227	0.002485	0.000825	0.000156	1.24E-05	2.46E-07	5.57E-10
	Lognormal	1.065571	0.747028	0.448851	0.213415	0.070807	0.013432	0.001062	2.12E-05	5.02E-08
	Nakagami-m	0.033414	0.023425	0.014075	0.006692	0.00222	0.000421	3.33E-05	6.63E-07	1.50E-09
	Negative Exp	0.01241	0.0087	0.005227	0.002485	0.000825	0.000156	1.24E-05	2.46E-07	5.57E-10
	Rice	0.01241	0.0087	0.005227	0.002485	0.000825	0.000156	1.24E-05	2.46E-07	5.57E-10
4-PAM	Gamma-gamma	0.266124	0.250755	0.231804	0.208719	0.181135	0.149162	0.113842	0.077672	0.044798
	Rayleigh	0.03628	0.034184	0.031601	0.028454	0.024693	0.020335	0.01552	0.010589	0.006107
	Lognormal	3.115177	2.935263	2.713428	2.443206	2.120315	1.746049	1.332598	0.90921	0.52439
	Nakagami-m	0.097684	0.092042	0.085086	0.076613	0.066488	0.054752	0.041787	0.02851	0.016443
	Negative Exp	0.03628	0.034184	0.031601	0.028454	0.024693	0.020335	0.01552	0.010589	0.006107
	Rice	0.03628	0.034184	0.031601	0.028454	0.024693	0.020335	0.01552	0.010589	0.006107

Authors' information

Yuvita Dian Safitri graduated from Politeknik Negeri Semarang, Indonesia, with S.S.T. degree in telecommunication engineering in 2017 and from University of New South Wales, Sydney, Australia, with an MEngSc in space systems engineering in 2024. She was employed as an engineer at the National Institute of Aeronautics and Space's (LAPAN) Remote Sensing Technology and Data Centre from 2018 to 2021. She has been employed with the National Research and Innovation Agency (BRIN) since 2021. Her areas of interest in research are space systems and ground station development. E-mail: *yuvita.dian.safitri@brin.go.id* ORCID ID: https://orcid.org/0009-0005-5190-0732

Ali Syahputra Nasution received the S.T. degree in telecommunication engineering from the Sekolah Tinggi Teknologi Telkom, Bandung, Indonesia, in 2005 and the M.T. degree in electrical engineering from University of Indonesia, Depok, Indonesia, in 2020. From 2008 to 2021, he worked as an Engineer at Remote Sensing Technology and Data Center, National Institute of Aeronautics and Space (LAPAN). From 2021 to the present, he has been working in National Research and Innovation Agency (BRIN). His research interests include remote sensing ground station development, error control coding, signal and image processing, as well as data hiding application.
E-mail: *alis003@brin.go.id* ORCID ID: https://orcid.org/0000-0003-2135-0782

Suhermanto received a Graduate degree in Electrical Engineering from the Universitas Gadjah Mada, The Special Region of Yogyakarta, Indonesia, in 1986 and the Magister degree in Optoelectrotechnics and Laser Applications from University of Indonesia, Depok, Indonesia, in 1998. Now he works as researcher at the Research Center for Satellite Technology, National Research and Innovation Agency (BRIN). His research of interest is in the field of remote sensing data acquisition technology and standard data processing. E-mail: *suhe001@brin.go.id*

Hidayat Gunawan received the B.Eng. and the M.Eng. degree in Electrical Engineering from University of Kansai, Japan, in 1992 and 1994. From 1994 to 2021, he worked as an Engineer at Remote Sensing Technology and Data Center, National Institute of Aeronautics and Space (LAPAN). From 2021 to the present, he has been working in National Research and Innovation Agency (BRIN). His research interests include remote sensing ground station and data processing development. E-mail: *hida003@brin.go.id* ORCID ID: https://orcid.org/0009-0001-1926-4095

Dinari Nikken Sulastrie Sirin earned a Graduate degree in Electrical Engineering from the Universitas Gadjah Mada, The Special Region of Yogyakarta, Indonesia, in 2004 and a Magister degree in Electrical Engineering from the Universitas Indonesia, Depok, Indonesia, in 2022. From 2008 to 2021, she worked as an Engineer at Remote Sensing Technology and Data Center, the National Institute of Aeronautics and Space (LAPAN). From 2021 to the present, she has worked in National Research and Innovation Agency (BRIN), at the Research Center for Satellite Technology. She is involved in research activities on remote sensing ground station technology, antennas, and remote sensing data processing. E-mail: *dina005@brin.go.id*. ORCHID ID: https://orcid.org/0009-0001-2806-9048

Andy Indradjad received the S.Si. degree in Physics from the University of Indonesia, Indonesia, in 1999, the M.Eng. degree in Signal Information Processing from Beihang University, Beijing, China, in 2011, and the Dr. degree in Physics from University of Indonesia, Indonesia, in 2024. From 2005 to 2021, he worked as an Researcher at Remote Sensing Technology and Data Center, National Institute of Aeronautics and Space (LAPAN). From 2021 to the present, he has

been working in National Research and Innovation Agency (BRIN). His research interests include remote sensing ground station development, system automation, signal and image processing. E-mail: andy003@brin.go.id ORCID ID: https://orcid.org/0000-0003-1269-0603

Supriyono received the BSc . degree in Applied Physics from University of Indoesia , Depok, Indonesia, in 1991 and the M.T. degree in Electrical Engineering from University of Indonesia, Depok, Indonesia, in 1998. From 1991 to 2021, he worked as an Weather Modification Technical Unit, The Agency for the of Assesment and Application of Technology (BPPT). From 2021 to the present, he has been working in National Research and Innovation Agency (BRIN). His research interests include remote sensing ground station development, telemetry, signal and image processing, software defined radio for receiving satellite data. E-mail: supr010@brin.go.id ORCID ID: https://orcid.org/0009-0009-2820-1254

Ahmad Maryanto received S.Si. degree in Physics from Universitas Gadjah Mada, Yogyakarta Indonesia, in 1993 and M.T. degree in Opto-Electrotechniques and Laser Application from Universitas Indonesia, Jakarta, Indonesia, in 2004. From 1994 to 2021, he worked as an Engineer at Remote Sensing Technology and Data Center, National Institute of Aeronautics and Space (LAPAN). From 2021 to the present, he has been working in National Research and Innovation Agency (BRIN). His research interests include remote sensing sensor development, geometric and radiometric processing of remote sensing imagery, calibration and validation of remote imaging data as well as all about reflectance spectroscopy. E-mail: ahma005@brin.go.id ORCID ID: https://orcid.org/0009-0009-8425-0587

Musyarofah received the degree in Physics from the IPB University, Bogor, Indonesia, in 2004 and the master degree in Geodesy and Geoinformation Science from Technische Universität Berlin, Germany, in 2020. From 2008 to 2021, she worked as a Researcher at Remote Sensing Technology and Data Center, National Institute of Aeronautics and Space (LAPAN). From 2021 to the present, she has been working in National Research and Innovation Agency (BRIN). Her research interests include remote sensing acquisition technology and data processing, and remote sensing signal and image processing. E-mail: musyarofah@brin.go.id ORCID ID: https://orcid.org/0009-0003-3464-1420

Muchammad Soleh received the S.T. degree in Engineering Physics from the Muhammadiyah High School of Quality Technology in 2002, and the M.Eng. degree in Global Navigation Satellite Systems from Beihang University in 2014. From 2005 to 2021, he worked as an Engineer at Remote Sensing Technology and Data Center, LAPAN. From 2021-2024 he worked as a Coordinator of Survey Equipment Management at Directorate of Laboratory Management, Research Facilities and Science and Technology Park, BRIN. And from 2025 to the present, he has been working as an Engineer at Research Center of Satellite Technology, BRIN. His research interests include remote sensing ground station development, GNSS, signal and image processing. E-mail: much008@brin.go.id ORCID ID: https://orcid.org/0009-0003-3479-7572

Andrew Dempster is a Professor at the School of Electrical Engineering and Telecommunications, The University of New South Wales, Sydney, Australia. He got his PhD from Cambridge in 1995 and now is Director of the Australian Centre for Space Engineering Research (ACSER). His area of expertise expands in Satellite Navigation Systems, e.g GPS, satellite systems, space policy, satellite communications, remote sensing, signal processing, space and satellites, and space resources. His current research including all areas relevant to GPS receiver design and signal processing, including all new GNSS systems and signals, interference, multipath, and hardware optimisation. New location technologies such as Locata and WiFi. Developing GNSS reflectometry for space and airborne platforms. Developing space resources, specifically the Wilde project. E-mail: a.dempster@unsw.edu.au ORCID ID: https://orcid.org/0000-0003-0881-1548

Received February 13, 2025. The final version – April 30, 2025.